CFD project PhD student group VT2020/2

Lea Miko Versbach,
William English, Xiaoqiang Zhang, Francesco Pignatelli

June 8, 2020

Abstract

In this report we investigate a ventilation system for sugar beet clamps which is currently under development in Sweden and Denmark. Sugar beets are stored post-harvest for up to two months. In order to avoid quality loss in the sugar beets, a ventilation system has been developed. With the use of CFD we model this ventilation system and study the air velocity as well as temperature. In the case of airflow, we compare the results to field studies.

1 Introduction

We are four PhD students with the following backgrounds:

- William English (Agricultural Science)
- Francesco Pignatelli (Mechanical Engineering)
- Lea Versbach (Numerical Analysis)
- Xiaoqiang Zhang (Heat transfer)

We are expected to choose a project which has a link to all of our research projects. We decided to use an application from William's project, using paper [2] as a reference point on how CFD methods can be applied to the ventilation of post-harvest stores of bulk commodity food crops.

1.1 Problem Description

Sugar beets in much of Europe are stored post-harvest in the field for periods of up to two months. They are stored in piles known as 'clamps', see Figure 1. While stored, the sugar beets maintain their life by consuming the sugar within their cells, in the biological process known as respiration. Moreover, they are attacked by fungal and bacterial pathogens. The rates of respiration and pathogen growth are temperature dependent. A general rule of thumb broadly adopted within the industry, is that the beets should not be stored in a clamp for more than 300 degree-days (°Cd); that is, for example, no more than 30 days at an average of 10°C, or 60 days at an average of 5°C, etc. The ideal clamp temperature is around 2 - 4°C. Air temperatures at the time of storage are commonly between 0 and 10°C, but can also be below 0°C for successive days.

Figure 1: Clamps of sugar beets and ventilation system (*source*: William English)

At stable temperatures and low wind speeds, modern uncovered A-structure clamps are usually around 10% warmer than the ambient air owing to respiration being exothermic.

When covered, convection process between a clamp and the ambient air can be greatly reduced. This means that following a drop in ambient air temperature, a clamp can be 5 to 10°C warmer than ambient air for a number of days. Conversely, should a covered clamp be cool, when the ambient air increases in temperature, the covered clamp can maintain a low temperature for a number of days. The need for covering clamps to keep out rain and the economic value of long-term storage has driven industry to start investigating possibilities for slowing the accumulation of degree-days. Actively ventilating clamps such that they are cooled when the ambient temperature is less than that of the clamp is one such possibility.

This project will apply CFD simulations to analyze one such ventilation system that is under development in Sweden and Denmark. The CFD simulations are carried out in ANSYS. A limited amount of experimental airflow data is available from the physical system to compare the computational results to.

1.2 Idea of the Project and Structure of the Report

Any clamp ventilation system should ideally distribute air through the clamp such that it is cooled quickly and evenly. The system that is herein investigated has not been developed primarily from this stand-point, but from a practical stand-point; that is, within the constraints of the practices a farmer normally undertakes, and the machinery that is normally available to them. As such, it may not be the ideal from a thermodynamic or fluid dynamic perspective. The idea of this project is thus to use CFD simulation to study the most important parameters in the clamp ventilation process, namely air velocity and temperature. From this, it may be possible to explain experimental results from tests that have applied the physical system without knowledge of the actual air flow from it, including with different system arrangements than those presented in this work. It will also be possible to test different designs of the physical system much more safely and cheaper than with experimental methods.

In Chapter 2 we study the velocity in the system. The model system consists of a main pipe with three outlet pipes (the metal pipes in Figure 1), which each have six pairs of outlet holes. Since the geometry becomes very big, we do not perform a mesh independence study here. While investigating velocity, we test different numerical methods and different turbulence models, namely k-ϵ, k-ω and RSM with Upwind and QUICK schemes. The results of this investigation are compared to the experimental data for the system [1]. Since this reference data is fully experimental and no computational reference results exists, we expect some differences.

In Chapter 3 we consider a heat transfer case. This is a hypothetical yet relevant study. We investigate the part of the ventilation system not covered by the clamp and how the ambient temperature can influence the air temperature inside this part of the ventilation system. By excluding the pipe parts that are covered by sugar beets, we can consider a simplified and ultimately symmetric geometry. This simplified geometry permits us to perform a mesh independence study. We study two arrangements of the system; with three, and with six of the smaller diameter outlet pipes.

2 Case study: Air velocity

In this chapter the air velocity in the ventilation system introduced above is studied. A 3D sketch of the system can be seen in Figure 2. The following assumptions for the computational model hold:

1. One main manifold pipe, and three outlet pipes each with six pairs of outlet holes,
2. One inlet with normal velocity of 23m/s,
3. The air flow is uniformly distributed between all i outlet pipes; in Figure 2, $i = 3$.
4. The air flow is uniformly distributed between the outlets i_j on any single outlet pipe; velocity at outlet i_1 = velocity at outlet $i_2 = \ldots$ = velocity at outlet i_j.

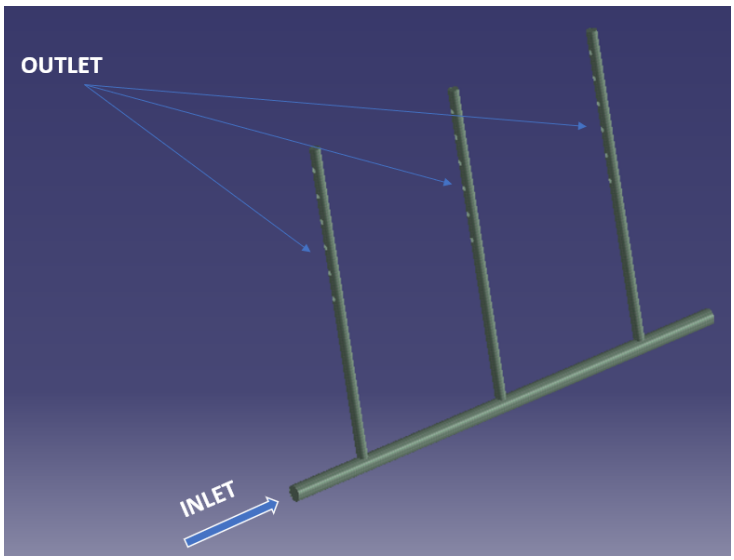

Figure 2: 3D CAD geometry

The true ideal shape of the air flow distribution across the outlets is not known. It is assumed to be dependent on the architecture of the clamp, but is beyond the scope of this project. We compare the distribution obtained from the CFD model to experimental results from field studies for the physical system [1].

2.1 Mathematical model

The airflow can be described by considering the flow as incompressible; in this case $Ma < 0.3$ since the inlet velocity (23 m/s) is much lower than the speed of sound in standard conditions (approximately 332 m/s). This assumption is supported by our reference paper [2] and it leads to air density changes affected only by buoyancy forces.

The flow studied is unavoidably affected by turbulence due to the fact that the actual Reynolds number Re is higher than the critical value Re_c, thus inertial forces are much more higher than the viscous ones. The presence of turbulence forced us to model the Reynolds stress tensor related to velocity fluctuation. Since we perform RANS simulations, it is assumed that the fluid respects the Boussinesq assumption.

Boundary conditions are set at one inlet and several outlets as shown in Figure 2. Moreover, numerical methods for the given problem have to be chosen. The latter two choices we make are presented in Sections 2.4 and 2.5.

2.2 Geometry

The geometry seen in Figure 2 is of the following dimensions:

- One inlet to the left.
- One, straight, 300 mm diameter manifold joining the inlet to the outlet pipes.
- Three parallel outlet pipes of 200 mm diameter and six meters in length, separated by three meters.
- Six pairs of outlet holes per outlet pipe. The outlet holes are 60 mm in diameter, 500 mm apart, and sit at 120° and 240° from the top of the pipe when lying.

For the calculations it is assumed that the geometry only consists of the fluid domain. In the physical system, the outlet pipes are 2 mm spiral welded steal, the manifold is a flexible cloth pipe, and these are joined by 1 mm stainless steel T-junctions.

2.3 Meshing and Mesh Independence Analysis

An unstructured mesh is applied. This permits easier generation for the complex given geometry, including refinements. The cost is that it requires more storage memory.

The element size is chosen to equal 10 mm and all geometry holes are refined with a face sizing element equal to 5 mm. This refinement is introduced in order to represent the flow at the outlet in the most accurate possible way. This choice is motivated by the fact that we extract data from those surfaces and compare it to experimental data. In order to represent the boundary layer trend close by the walls in the best way possible, ten inflation layers with a growth rate equal to 1.2 are set.

In Figure 3 the aspect ratio, orthogonal quality and skewness parameters for the given mesh are shown. By comparing the obtained values with the reference ones provided in the course lectures, it is possible to claim that we can be satisfied with the orthogonal quality and the skewness since they are quite close to the reference one. On the other hand, the aspect ratio parameter is unfortunately quite far from being equal to one. This can cause problems with numerical stability and accuracy of the solution. Fortunately, the problematic elements are confined on the top of the small outlet pipes, close to the flow stagnation point, which is not very interesting for our analysis.

Since the model becomes very big, we decide to run a mesh independence analysis only on the simplified geometry for the heat transfer case, see Section 3.3. Even with the full license ANSYS version, the problem becomes computationally heavy and therefore the mesh independence analysis is outside of the scope of the Air velocity case. However, given the results of that section, we are confident that the mesh used here is of a high enough resolution to provide solutions that are not negatively impacted by it.

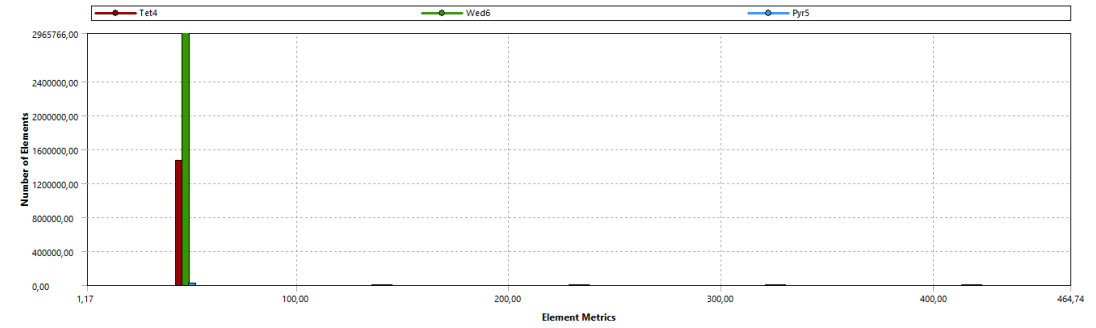

(a) Aspect ratio

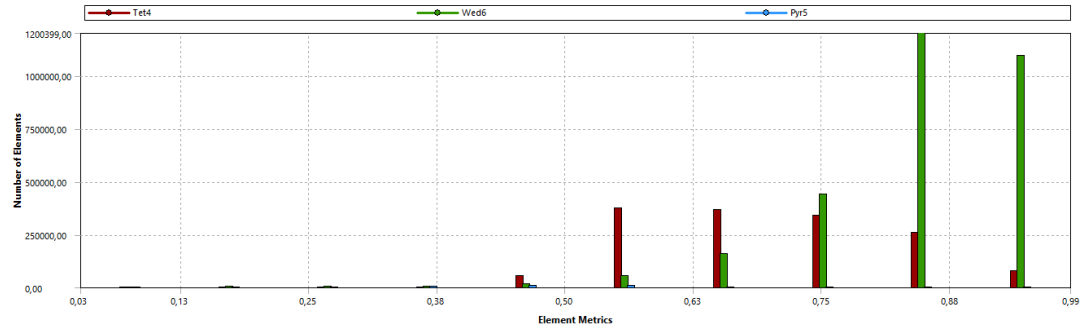

(b) Orthogonal quality

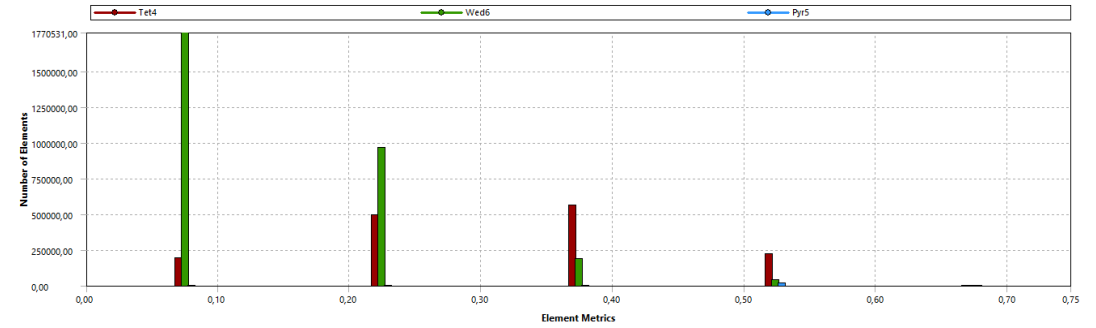

(c) Skewness

Figure 3: Results meshing the full geometry with element size 0.05 m and refinement mesh size of 0.01 m at the small long pipes and 0.005 m at the inlet and outlet holes

2.4 Models and Methods

The energy equation is solved using one numerical scheme, namely a first order finite volume discretization, which is a commonly chosen method in CFD. The problem is solved without the energy equation, using different numerical schemes in order to investigate their influence on the solution. All results are produced using the full ANSYS version.

Three different turbulence models are considered: Standard $k-\epsilon$, Standard $k-\omega$ and RSM, with both QUICK and Upwind numeric schemes to solve these equations. Both $k-\epsilon$ and $k-\omega$ are two-equations RANS turbulence models based on the Boussinesq's hypothesis. This introduces a new variable, the so-called turbulent viscosity, while expressing the Reynolds stress anisotropy as a linear function of the mean velocity gradients. The two numeric schemes are reliable in managing steady convective-diffusion problems. It is also possible to use Central Difference schemes, but this requires assumptions and further analysis on the Peclet Number ($Pe < 2$) in order to avoid wiggles.

Let k be the turbulent kinetic energy, ϵ the dissipation rate of the turbulent kinetic energy and ω the vorticity. The two RANS models express the turbulent viscosity ν_t as a function of k and ϵ in the first case and k and ω in the second one.

- k-equation

$$\frac{\partial k}{\partial t} + \overline{u}_j \frac{\partial k}{\partial x_j} = P - \epsilon + \frac{\partial}{\partial x_j}[(\nu + \frac{\nu_T}{\sigma_k})\frac{\partial k}{\partial x_j}] \tag{1}$$

- ϵ-equation

$$\frac{\partial \epsilon}{\partial t} + \overline{u}_j \frac{\partial \epsilon}{\partial x_j} = C_{\epsilon 1}\frac{\epsilon}{k}P - C_{\epsilon 2}\frac{\epsilon^2}{k} + \frac{\partial}{\partial x_j}[(\nu + \frac{\nu_T}{\sigma_k})\frac{\partial \epsilon}{\partial x_j}] \tag{2}$$

- ω-equation

$$\frac{\partial \omega}{\partial t} + \overline{u}_j \frac{\partial \omega}{\partial x_j} = C_{\omega 1}\frac{\omega}{k}P - C_{\omega 2}\omega^2 + \frac{\partial}{\partial x_j}[(\nu + \frac{\nu_T}{\sigma_k})\frac{\partial \omega}{\partial x_j}] \tag{3}$$

Since the Standard $k-\epsilon$ model usually has issues in handling strongly curved streamlines and sudden changes on the flow direction, $k-\omega$ is considered as well.

The RSM turbulence model is quite different from the previous mentioned models since it is not based on the Boussinesq's hypothesis but on the following equation:

$$\frac{\overline{D}}{\overline{D}t}\overline{u_i' u_j'} + \frac{\partial}{\partial x_k}T_{kij} = P_{ij} + R_{ij} - \epsilon_{ij}, \tag{4}$$

with

- T_{kij} the turbulence and pressure transport term,
- P_{ij} the turbulence production term,
- R_{ij} the pressure-rate-of-strain term,
- ϵ_{ij} the turbulent dissipation term.

Each of these terms have to be modelled. In a 3D case this results in seven model equations. Boundary layer flow behaviour can be a signficant issue for $k-\epsilon$ models (this is neither a problem for $k-\omega$ nor for RSM) and is usually treated in one of two ways:

1. y^+ control that must be equal or lower than 1 (it should drop into the viscous sublayer zone). Achievement of this constrain requires a very fine mesh close to the wall. Then turbulence is solved in the viscous sub layer zone as well.

2. Usage of so-called wall functions which model the near wall region. These are empirically derived equations that satisfy the physics in the near wall region and represent some connection between the wall and the fully developed turbulence zone. This avoids the need of solving the boundary layer.

In the current case, "wall function" are enabled since we could not afford to refine the mesh close by the wall to get $y^+ < 1$ due to computational power limits and available time.

The QUICK scheme (abbreviation for Quadratic upstream interpolation for convective kinetics) is a higher-order differencing scheme that considers a three-point upstream weighted quadratic interpolation for the cell face values:

$$\phi_e = \phi_P + \frac{1}{8}(3\phi_E - 2\phi_P - \phi_W).$$

The diffusive terms are evaluated from the gradients of the parabola coming from the quadratic interpolation. It fulfills conservativeness and transportiveness, but not the boundedness property since under- and overshoots are produced. The scheme is only conditionally stable, which can be improved by reformulating the scheme. QUICK is more accurate than pure upwind schemes, namely 3rd order on uniform meshes.

The upwind differencing scheme is based on computing the convective term depending on the flow direction. In the scheme it is assumed that the value at a face is equal to the value at the cell center in the cell upstream to the face, i.e.

$$\phi_e = \phi_P.$$

The scheme is very diffusive and only of 1st order, but it fulfills the properties of conservativeness, boundedness and transportiveness.

SIMPLE is used to solve the equation system; this method is a staggered grid based method that resolves the coupling between velocity and pressure problem in incompressible flow cases.

Combining the methods with the two different schemes, we have in total six solvers to test and compare for the air velocity case.

2.5 Boundary Conditions

Dirichlet boundary conditions are set at the inlet. In the physical system, air is pumped into the pipe system using a centrifugal fan operating at 50 Hz, which may produce an uneven velocity distribution in the flow. Given the length of manifold before the first outlet pipe, we expect the velocity distribution to have normalised. Thus for simplicity, it

is assumed that air enters the system with a linear velocity profile (normal velocity equal to 23 m/s).

On the outlets Dirichlet boundary conditions are set as well, by assigning the atmospheric pressure on them. All parts of the fluid domain in contact with the solid wall are defined with no slip wall boundary conditions, i.e. the velocity is assumed to be equal to zero. Due to the non-symmetric shape of the system it is not possible to simplify the geometry and to assign symmetry boundary conditions.

2.6 Solution

Each of the six solver methods described are run with a tolerance $1e-6$ and a maximum of 1000 iterations. Convergence is not reached with any of the methods, as can be seen in Figure 4, but we decided to not increase the number of iterations since the cases started to become very expensive to save.

2.7 Results and discussion

In general, the $k-\epsilon$ model works best and the RSM model returns the worst results in terms of accuracy, even if RSM seems to be more stable. Moreover, Upwind schemes give slightly better residuals for all three methods than QUICK schemes. It can be seen in all residual plots that the continuity equation is most problematic to solve and its solution is affected by a lower accuracy.

In Figure 5 the pressure contour plots are presented. The pressure decreases towards the outlets; this is what we expected.

The velocity stream lines can be seen in Figure 6. As expected, the velocity decreases towards the right and along the outlet pipes. Only at the T-junctions, where the air is entering the outlet pipes, is an increased velocity noted. This is caused by the turbulence produced by the geometry, which can be seen in Figure 7. The turbulence kinetic energy increases at the T-junctions and at the outlets.

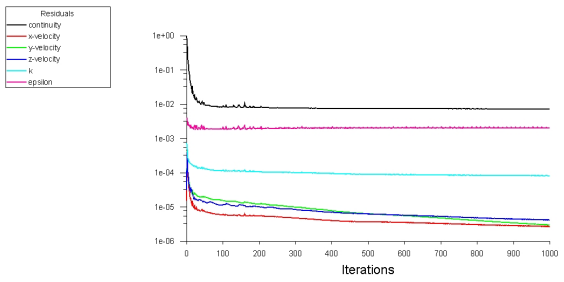

(a) $k-\epsilon$ with QUICK

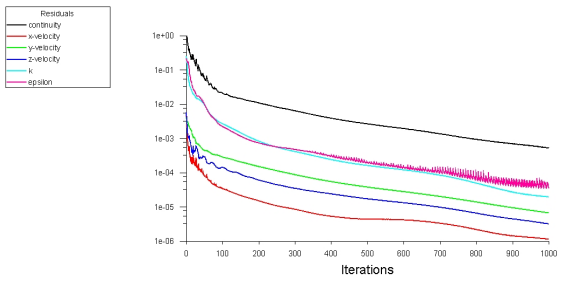

(b) $k-\epsilon$ with Upwind

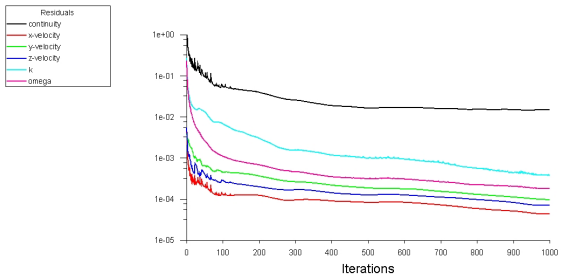

(c) $k-\omega$ with QUICK

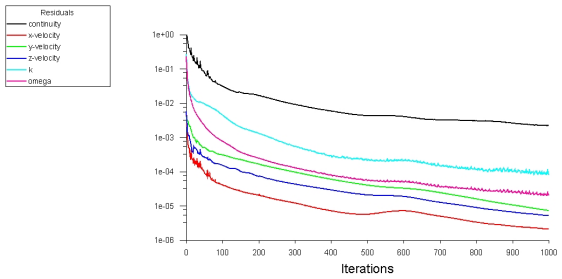

(d) $k-\omega$ with Upwind

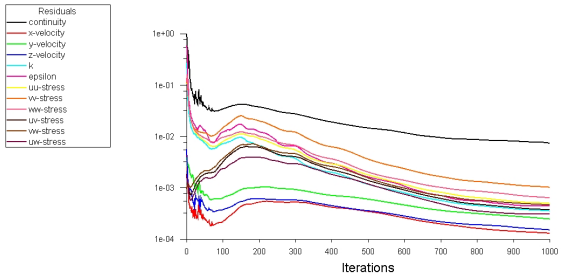

(e) RSM with QUICK

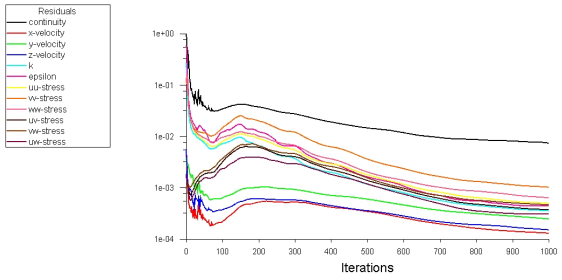

(f) RSM with Upwind

Figure 4: Residual for different numerical methods

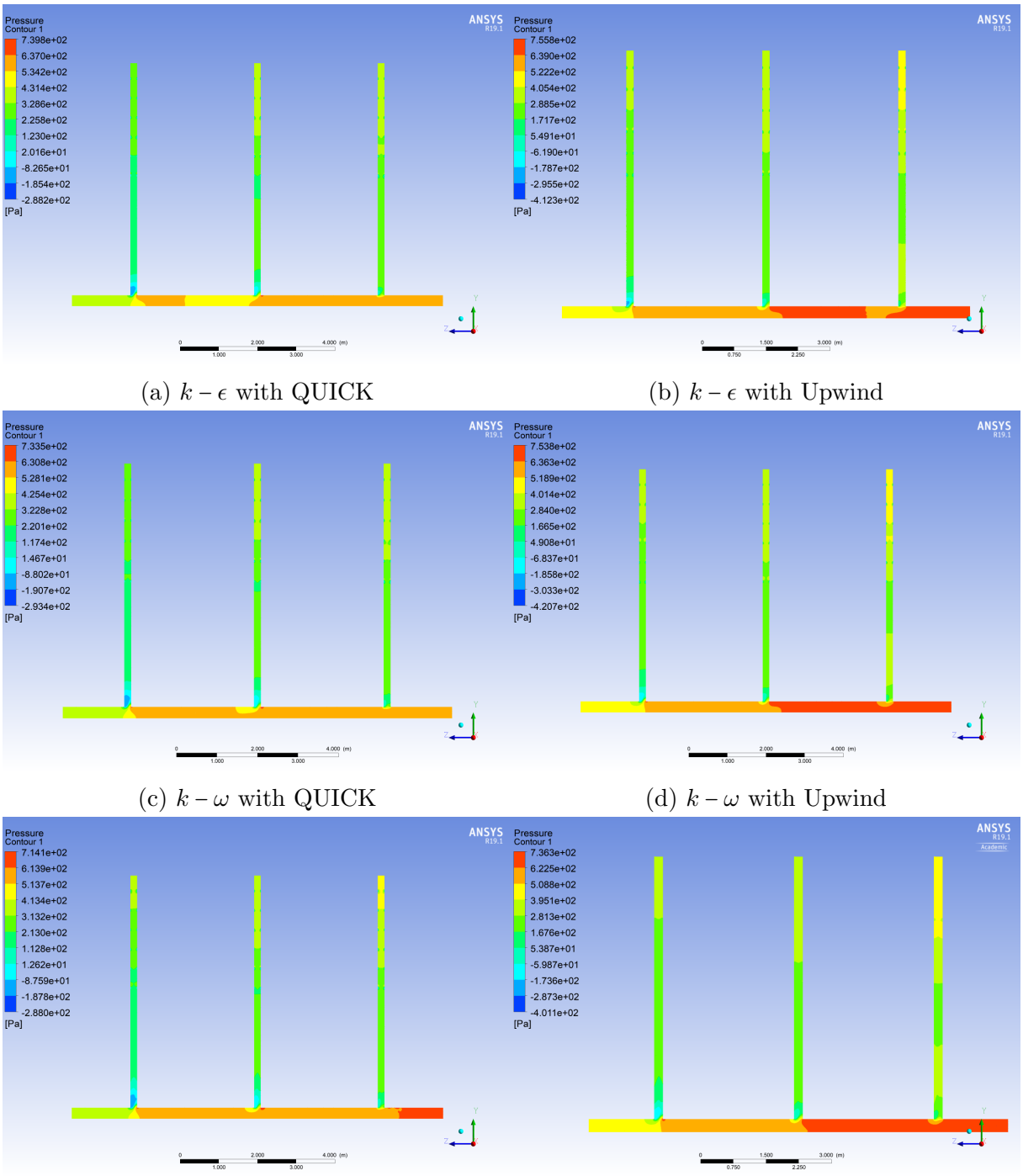

(a) $k-\epsilon$ with QUICK

(b) $k-\epsilon$ with Upwind

(c) $k-\omega$ with QUICK

(d) $k-\omega$ with Upwind

(e) RSM with QUICK

(f) RSM with Upwind

Figure 5: Pressure contour plot for different numerical methods

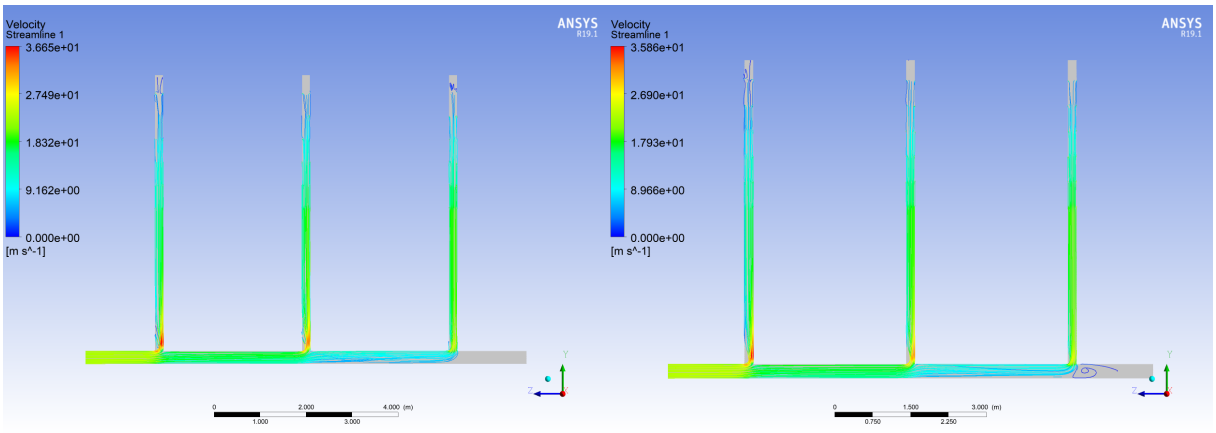

(a) $k-\epsilon$ with QUICK

(b) $k-\epsilon$ with Upwind

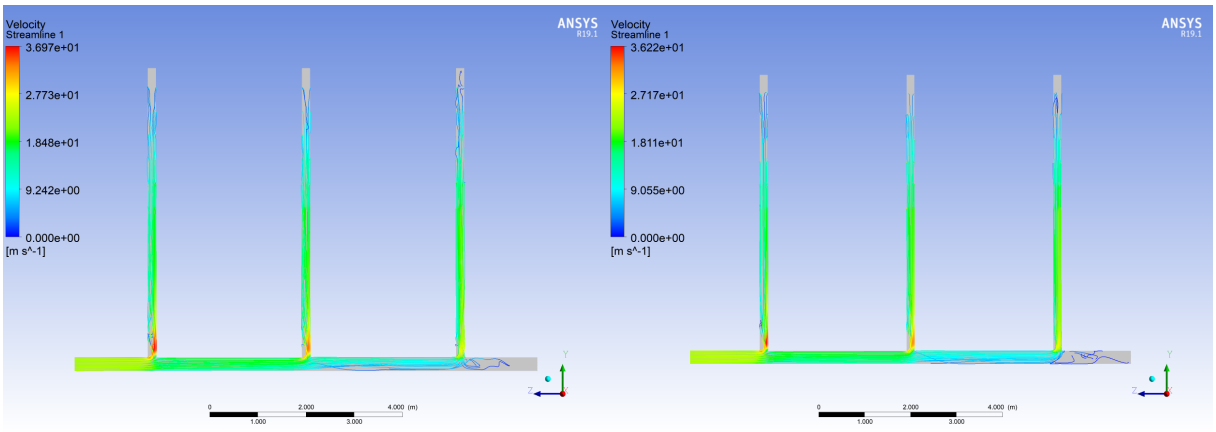

(c) $k-\omega$ with QUICK

(d) $k-\omega$ with Upwind

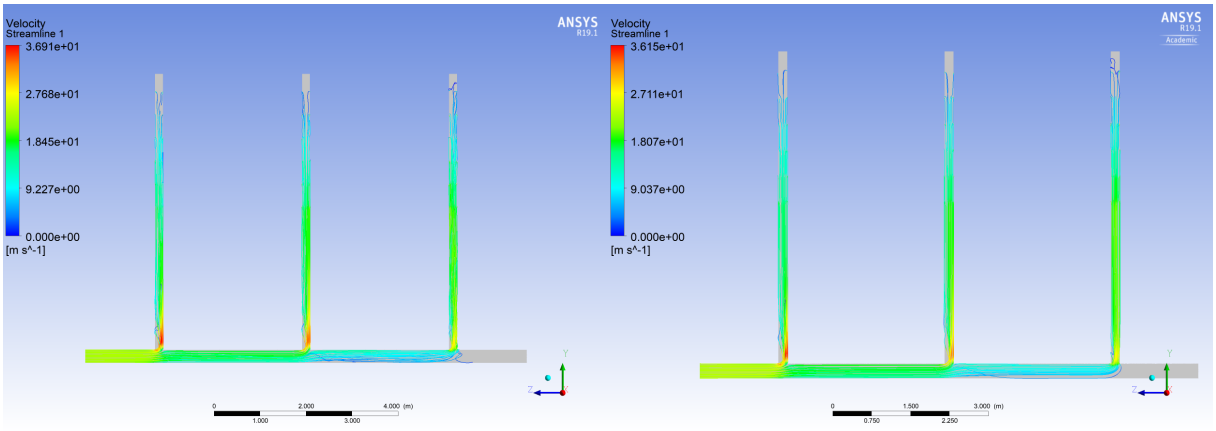

(e) RSM with QUICK

(f) RSM with Upwind

Figure 6: Velocity stream lines for different numerical methods

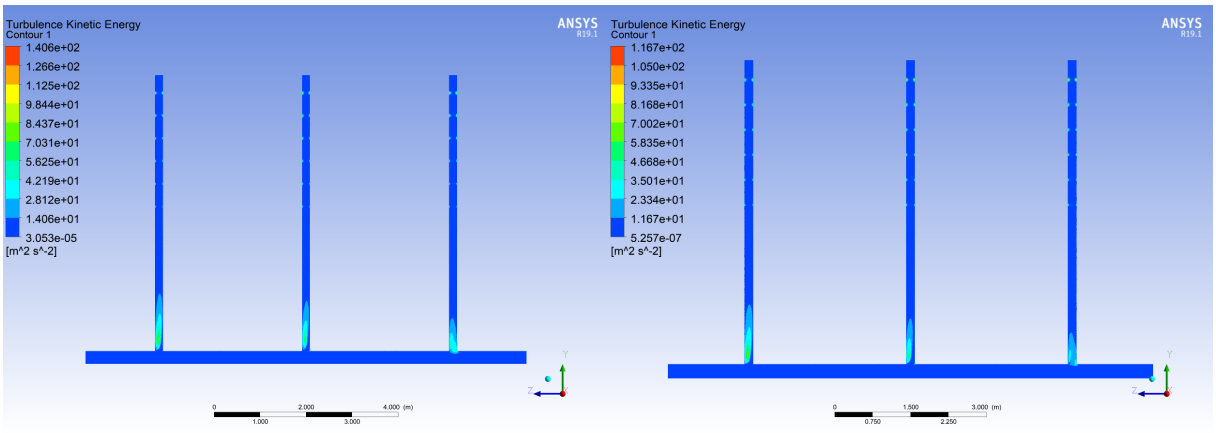

(a) $k-\epsilon$ with QUICK (b) $k-\epsilon$ with Upwind

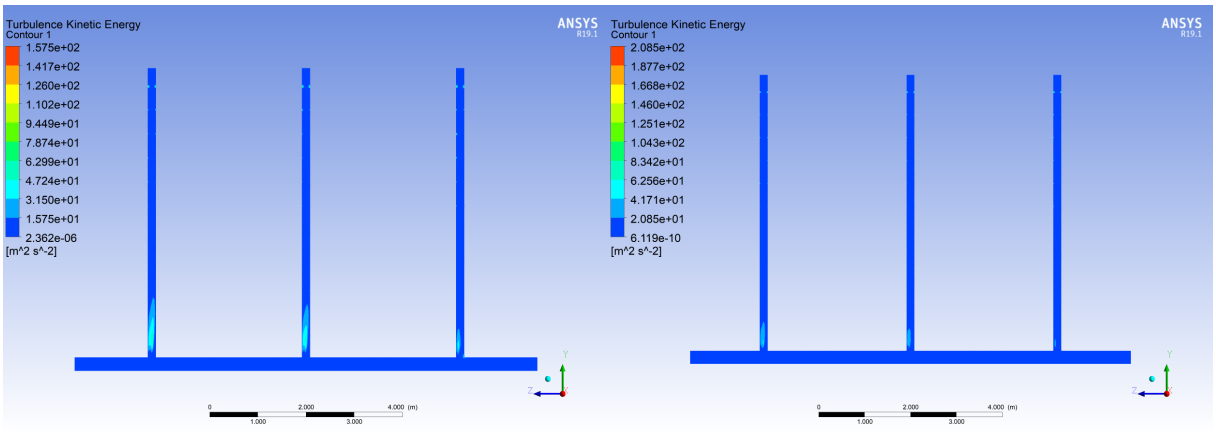

(c) $k-\omega$ with QUICK (d) $k-\omega$ with Upwind

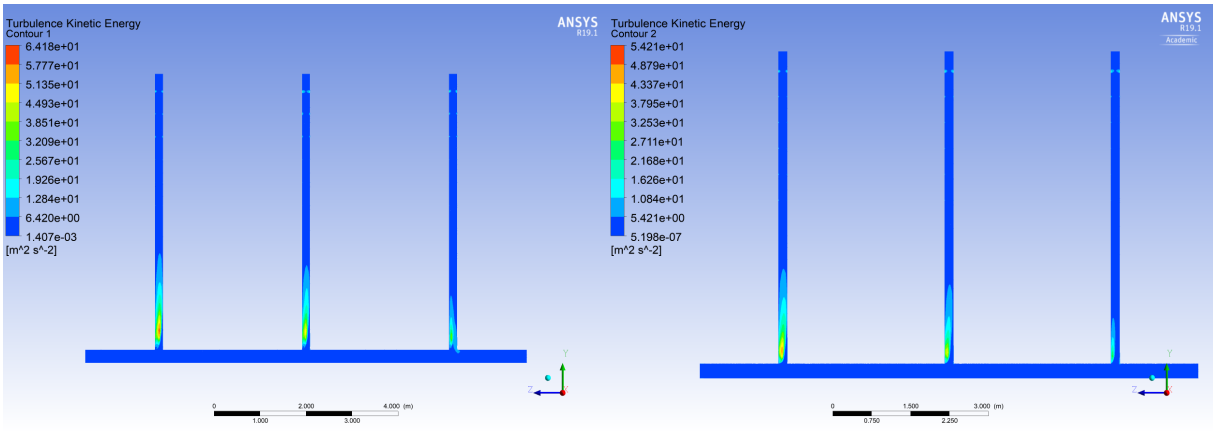

(e) RSM with QUICK (f) RSM with Upwind

Figure 7: Turbulence kinetic energy for different numerical methods

2.8 Comparison to Measured Results

We now compare the results obtained by the CFD model to experimental field results collected by William. Table 1 and Figure 8 present the velocities for the system at the outlet holes. Both the computed velocities for the RSM model with upwind, and the experimental value as measured in the field, are shown [1]. Values are presented as the average of the pairs of outlet holes, with Outlet pair 1 being the pair closest the inlet. Pipe 1 is that closest the inlet. We have chosen to show the results from the RSM model since it is the most stable, even if it is also less precise.

Outlet pair	Model			Experimental		
	Pipe 1	Pipe 2	Pipe 3	Pipe 1	Pipe 2	Pipe 3
1	24.7	23.6	20.4	20.0	21.2	22.0
2	24.8	23.8	20.9	21.2	22.5	23.3
3	24.9	24.0	21.1	22.2	23.5	24.5
4	24.9	24.3	21.5	23.0	24.2	25.4
5	25.3	24.9	23.6	23.7	24.9	26.2
6	25.4	25.2	22.4	24.1	25.7	26.5

Table 1: Model and Experimental velocities (m/s) at pairs of outlet holes

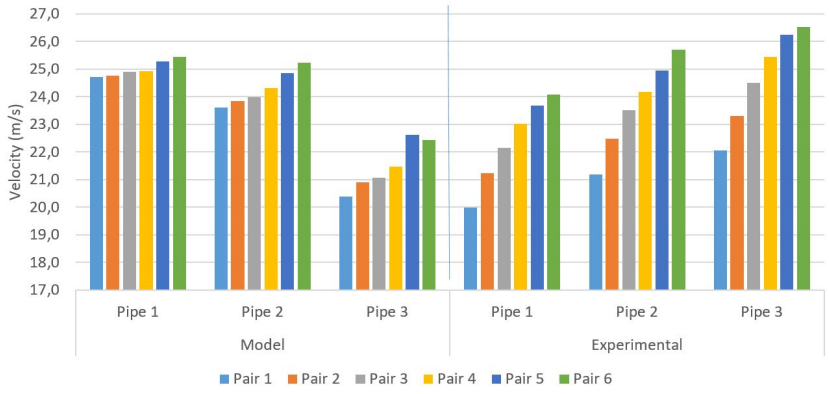

Figure 8: Model and Experimental velocities (m/s) at pairs of outlet holes

There are both similarities and differences between the two sets of results. Regarding similarities, the total volume of air passing through the systems, measured as the average velocity over all outlets, is identical to one decimal place. Further, the values from both sets of results increase with the distance along any one outlet pipe; that is, Outlet pair velocities are ranked Outlet pair 6 > ... > Outlet pair 1 for both sets of results.

The most stark difference is that the experimental outlet pipe average values increase with distance from the inlet, while the model showed the inverse. A second difference is not shown in the presented data, but the experimental velocities appear more similar within any pair than for those gained from the model. These differences can possibly be explained by the fact that the assumptions for the mesh are not good enough to match the experimental results, but as explained before, there existed computational limitations when refining the mesh.

3 Case study: Heat Transfer

We now present a case in which a hypothetical yet realistic heat transfer scenario is investigated. This case builds on the Air velocity case, in that it takes the same system and geometry as its starting point. It applies the same mathematical model assumptions, and the models and method the Air velocity case deemed most appropriate for this system. We perform a mesh independence analysis for this case.

3.1 Case study problem

This heat transfer case study focuses on the sections of the system that sit in the open air, namely the manifold and the first 30 cm of the outlets pipes. These sections are subjected to a negative degrees Celsius temperature (-4°C), while at the same time a heater is placed at the inlet so that a positive degrees Celsius temperature (+4°C) enters the system. The case investigates whether the air entering the clamp maintains a positive temperature. This is a scenario that is being considered as a means of helping the stored sugar beets cope with prolonged periods of sub-zero temperatures.

Two arrangements of the system are presented:

- 3 x 3 - three outlet pipes with a three meter separation; the same as in the case above.
- 6 x 3 - six outlet pipes with a three meter separation.

The 6 x 3 arrangement can be seen in Figure 9.

3.2 Geometry

The geometry for this case study is simplified to match the needs of the case. In the first instance and given it is only necessary to understand the temperature in the outlet pipes to the point of entering the clamp region and not at the outlets holes, the outlet pipes are shorted. As such, the outlet holes on the outlet pipes are removed and a symmetry is introduced to the body along the length of all pipes.

Originally, the geometry included just the 30 cm of the outlet pipes that sits in the open air. This, however, meant that issues with a reversed flow over the domain outlets materialise and persist over a calculation of 1000 iterations. By lengthening the outlet pipes to 100 cm, this issue no longer persists. A slice is placed along the outlets at 30 cm to permit the different wall boundary temperatures along these lengths. This cut can be seen in Figures 9 and 10.

The simplified geometries present the additional challenge of correcting for the non-equal pressure at the outlets, as would be present in the physical system at 100 cm along the outlet pipes. Using 0 Pa gauge pressure at the outlets in this case produces average velocities with a Pipe 1 : Pipe 2 : Pipe 3 ratio of approximately 1 : 1.26 : 1.52, while the experimental values are 1 : 1.06 : 1.10. An attempt to correct this is made by taking the average pressures at 100 cm along each of the outlet pipes in the above Air velocity case. The computed values are: Pipe 1, 282.68Pa. Pipe 2, 179.12Pa. Pipe 3, 123.51Pa. Application of these values to the simplified geometry only accentuated the issue. Noting

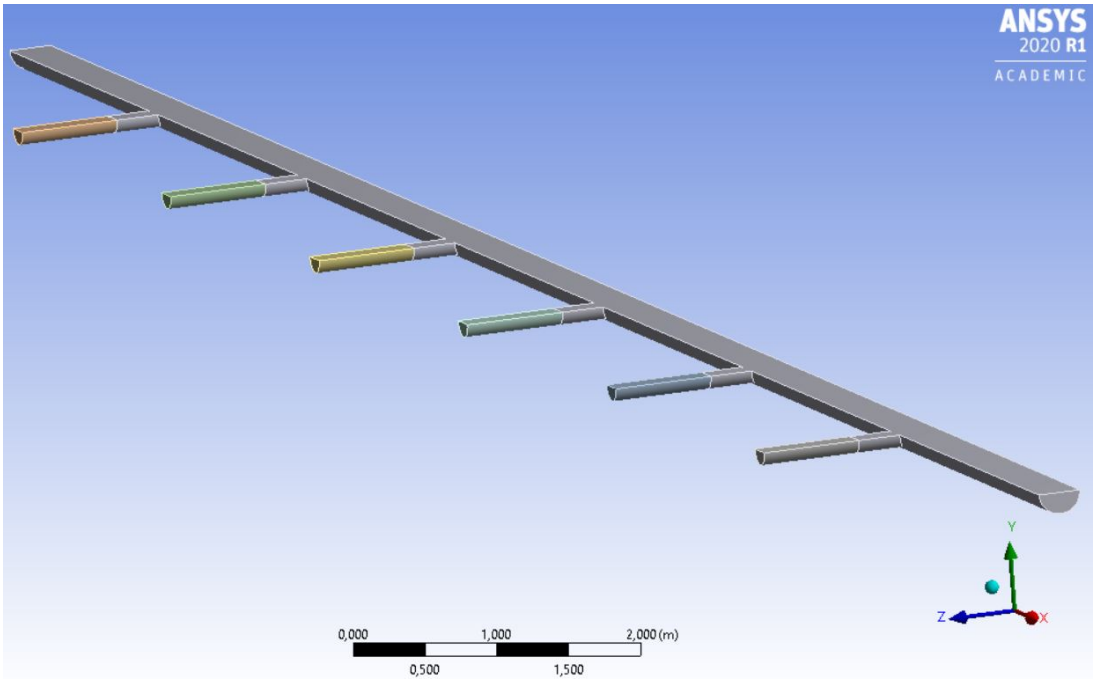

Figure 9: 3D geometry of 6 x 3 arrangement, with shortened outlet pipes

that in the Air velocity case, the model is returning outlet pipe average velocities in the reverse order to the experimental values, the computed pressure values from the Air velocity case are also reversed. The resulting application of these values as outlet gauge pressures in this Case results in the solution with a ratio of outlet velocities of 1 : 1.16 : 1.12. This is a marked improvement, especially when comparing outlet pipes 1 and 3.

Two issues, however, remain: the higher value at outlet pipe 2 than for outlet pipe 3 does not represent the physical system; and we do not have measured nor modelled values for the 6 x 3 arrangement. In light of these issues, it is decided to continue this Case with 0 Pa outlet gauge pressures rather than to complicate the comparisons between the the 3×3 and 6×3 arrangements, or to attempt to guess the required outlet gauge pressures.

3.3 Meshing and mesh independence analysis

To study the importance of mesh resolution and structure on a solution, a mesh independence analysis is conducted. This analysis is performed on this heat transfer case study as the simplified geometry allowed for higher resolutions to be tested with a lower computational cost. To further lower this cost, it is only conducted on the 3×3 arrangement. Constrains from the 6×3 geometry are taken to define the third of the 3×3 meshes, so as to test whether both arrangements could be run within the limits of the Academic licence. The independence analysis is conducted considering five meshes;

1. Baseline mesh, with program defaults.
2. Baseline mesh, with the inclusion of inflation. For the inflation, five layers are used, a smooth transition with transition ratio of 0.272, and a growth rate of 1.2 are applied. In comparison to the ten layers of the Air velocity case, only five layers are used primarily given the constraints on element number of the Academic licence.

3. Reduced element size mesh. The element size is taken to be that which in the 6 x 3 geometry would keep the total number of elements below the 512 000 constraint of the Academic licence in ANSYS. As such, body sizing with an element size of 0.0263 m is applied to the entire geometry.

4. Limiting mesh, with element size taken as that which keeps the 3 x 3 mesh within the 512 000 constraint of the Academic licence in ANSYS; body sizing with an element size of 0.0216 m is applied to the entire geometry.

5. Overkill mesh, with element size set to 0.0130 m.

	3 x 3					6 x 3
Mesh reference	1	2	3	4	5	3
Inflation (no. layers)	No	Yes (5)	Yes (5)	Yes (5)	Yes (5)	Yes (5)
Element size (m)	0.6334	0.6334	0.0263	0.0216	0.0130	0.0263
Nodes	10 285	31 004	96 590	160 538	479 328	174 603
Elements	35 710	69 595	282 040	505 197	1 607 435	508 431

Table 2: Mesh statistics

Figure 10 shows the mesh along one of the shortened outlet pipes and some of the manifold for Mesh 3: inflation layers = 5, element size = 0.0263 m.

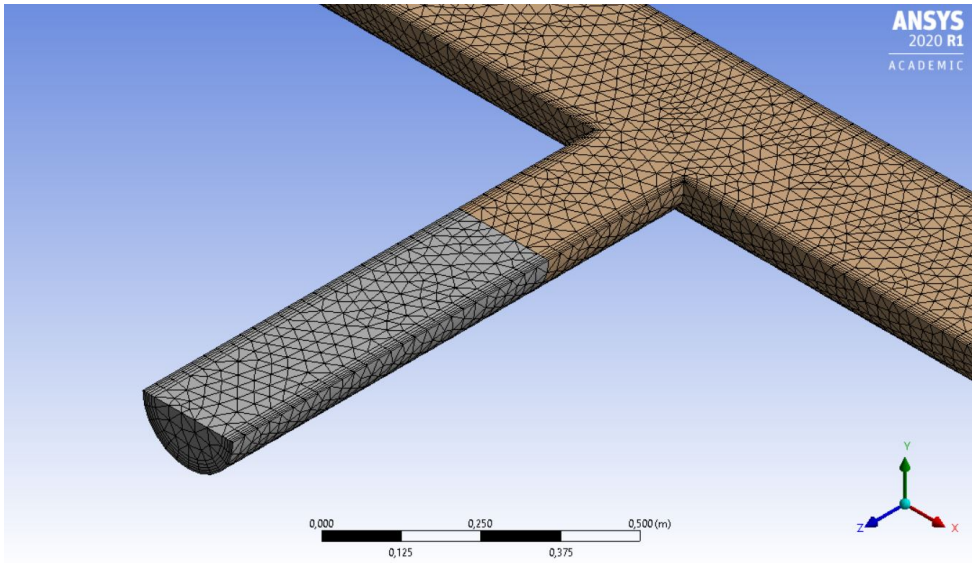

Figure 10: Mesh 3: inflation layers = 5, element size = 0.0263 m

Inflation is included in the mesh to improve the resolution along the walls, where both the heat transfer and turbulence are assumed to be most variable. Decreasing the elements size is similarly a strategy for improving the resolution and quality of the mesh at all points.

3.3.1 Mesh Independence Mesh quality

Mesh quality statistics, summarized in Table 3, show how the inclusion of inflation caused the overall quality of the mesh to reduce. In particular, the mean values for Element quality and Aspect ratio both moved in the direction of a poorer mesh. This is expected given wedge shaped elements are introduced with inflation. The wedge shaped elements are long and skinny, resulting in large aspect ratios. In general, the quality statistics improve again with successive decreases of element size. The difference between Mesh 3 and Mesh 4 is marginal on all parameters. It is interesting to note that the mesh quality statistics for Mesh 5 are quite similar to those of Mesh 1, despite the 45-fold increase in the number of element; this is the cost of inflation with regards quality statistics.

		3 x 3				
Mesh ref.		1	2	3	4	5
Element quality	Mean	0.829	0.535	0.639	0.665	0.862
	SD	0.010	0.251	0.261	0.255	0.010
Aspect ratio	Mean	1.878	4.204	3.4211	3.215	1.870
	SD	0.479	2.329	2.193	2.114	0.423
Skewness	Mean	0.243	0.234	0.188	0.187	0.207
	SD	0.126	0.127	0.117	0.120	0.122
Orthogonal Qual.	Mean	0.759	0.765	0.811	0.812	0.792
	SD	0.126	0.126	0.116	0.119	0.121

Table 3: Mesh quality statistics

3.3.2 Mesh Independence Models and Methods

Using these different meshes, the mesh independence analysis is conducted with the following parameters;

- Models:

  Turbulence: $k-\epsilon$, with Enhanced wall treatment.

  Energy: on.

- Boundary conditions:

  inlet: velocity 23 m/s, 300 K

  outlet: gauge pressure 0 Pa

  walls - external to clamp (manifold and 0-30 cm of outlet pipes): no slip, 280 K

  walls - internal to clamp (30 - 100 cm of outlet pipes): no slip, 300 K

- Method:

  Pressure-Velocity Coupling: SIMPLE

  Spatial Discretization: Gradient - Green-Gauss Cell Based, Pressure - Standard, Momentum / Turbulent Kinetic Energy / Turbulent Dissipation Rate - First Order Upwind, Energy - Second Order Upwind.

- Tolerance on residuals: $1.e^{-21}$.
- Maximum iterations: 1 000.

The model and methods are taken as those deemed most appropriate for this system in the Air velocity case, namely SIMPLE with Upwind. The temperatures for the boundary conditions in the mesh independence study are taken as slightly broader than those described above for this case study, so as to increase the variance and thus increase the strain on the computations slightly. NB: Mesh 5 is not included in the results owing to the restrictions of the Academic licence.

The statistics gained from each mesh are shown in table 4

	3 x 3			
Mesh ref.	1	2	3	4
Continuity residual	$2.61e^{-10}$	$1.12e^{-8}$	$3.19e^{-6}$	$2.95e^{-5}$
Energy residual	$5.29e^{-8}$	$8.52e^{-8}$	$1.85e^{-8}$	$1.22e^{-8}$
Iterations	1 000	1 000	1 000	1 000

Table 4: Mesh solution residuals

3.3.3 Mesh Independence Results

Figure 11 presents results of the velocity at the three outlets, on the symmetry plane, for meshes 1 to 4. These show that meshes 3 and 4 - the green and pink lines respectively - give very similar results.

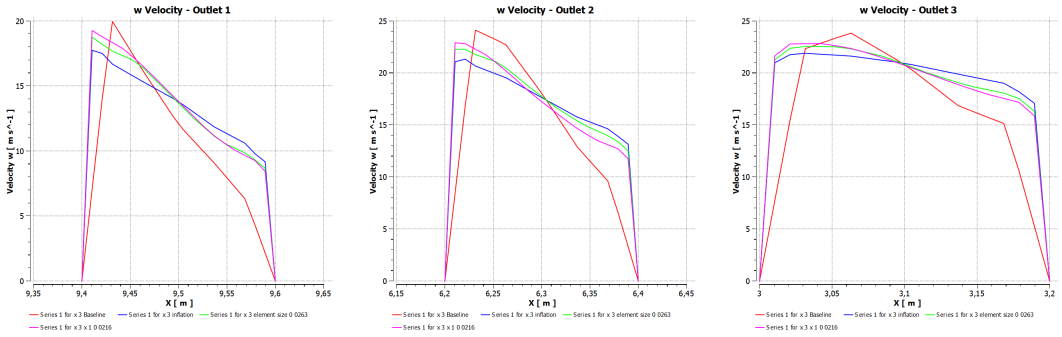

(a) Outlet 1 (b) Outlet 2 (c) Outlet 3

Figure 11: Velocity normal to outlet boundary, 100 cm along outlet pipe.

Figure 12 presents results of the temperature gradient along the symmetry plane at the T-junction of outlet pipe 3 - that furthest from the inlet. Again, Meshes 3 and 4 appear most similar. Given this case study's focus on temperature profiles, it is of some concern that Mesh 4 is showing slightly higher temperatures further along the manifold and outlet pipe than Mesh 3. It can be said that mesh 3 gives a more conservative result in terms of the risk in the application of this case in the physical system. When Mesh 3 is run to convergence at approximately 3 500 iterations (results not shown), the temperature

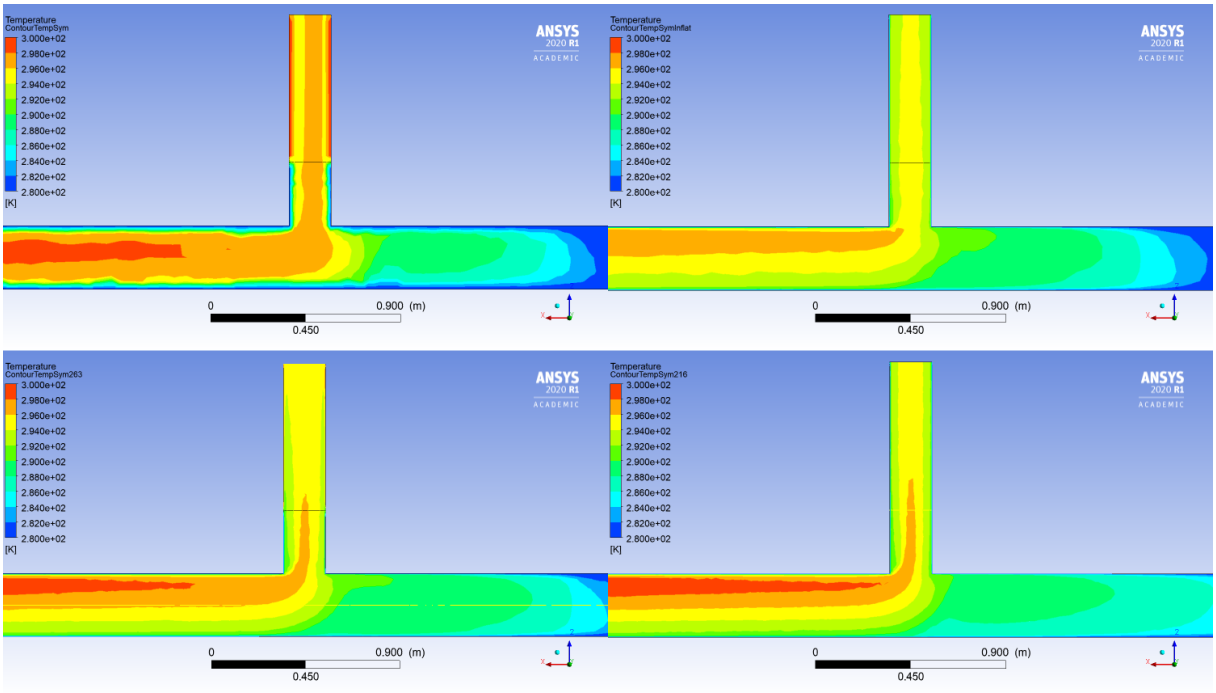

Figure 12: Temperature contours on symmetry plane, centered on 3rd outlet. Top left to bottom right: Mesh 1, Mesh 2, Mesh 3, Mesh 4.

profile is very similar to that of the 1 000 iteration run, suggesting the differences in the temperature profiles is a result of the meshes and not the number of iterations.

As a result of the mesh independence analysis, it is concluded that Mesh 3 is sufficient to use in the case study. While results are not stable between Mesh 3 and Mesh 4, the differences are small and support a conservative approach to risk. Thus, we conclude it is better to use Mesh 3 and be able to run both system arrangements than to take Mesh 4 and exclude the 6×3 arrangement.

Using the dimensions of Mesh 3 on both the 3×3 and 6×3 arrangement, the following setup is used to run the calculation of temperature across the domain for the Heat transfer case study.

3.4 Models and Methods

Models and Methods are chosen as described in the mesh independence study.

3.5 Boundary conditions

Following the conditions of the case as described in sections 3.1 and 3.2, the following boundary conditions are applied:

- Inlet: velocity 23 m/s, 277.15 K,
- Outlet gauge pressure: 0 Pa,
- Walls - external to clamp: no slip, 269.15 K,
- Walls - internal to clamp: no slip, 277.15 K.

3.6 Solution

Each arrangement is run with a tolerance $1e-21$ and a maximum of 4 000 iterations. Convergence is reached for the 3×3 arrangement on all residuals after approximately 3 500 iterations. For the 6×3 arrangement, convergence is only reached for the energy equation after 4 000 iterations.

3.7 Results

The temperature contour along the symmetry plane for the 3×3 arrangement (Figure 13a) suggests that there are no negative temperatures at any outlet. This is confirmed in Figure 14a, where it can be seen that the minimum temperature at 100 cm along the outlet pipes is on outlet pipe 3 - that furthest from the inlet - at approximately 1.70°C.

For the 6×3 arrangement, Figure 14b shows that the furthest outlet pipe from the inlet - the sixth outlet pipe - came very close to having a sub-zero temperature at 100 cm, with a minimum of 0.35°C. Inspecting Figure 15b shows that a sub-zero Celsius temperature seems to be present at 30 cm. The differences at the two locations can be attributed to the the heat from the beet pile between 30 cm and 100 cm.

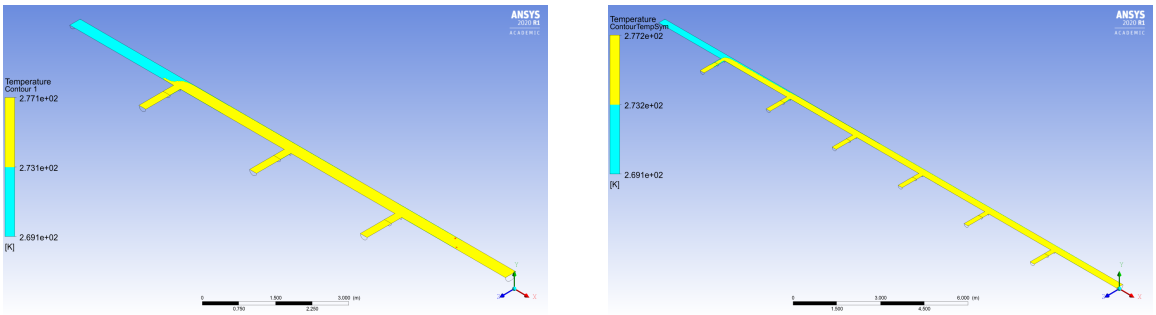

(a) 3 x 3 arrangement

(b) 6 x 3 arrangement

Figure 13: Contour of temperature over symmetry planes

3.8 Discussion

Overall, the model systems are able to deliver heated, positive degree Celsius air to the outlets, albeit with a small margin for error in the 6×3 arrangement. When this small margin of error is put in the context of the 0 Pa outlet gauge pressure as discussed in section 3.2, it is possible that a negative degree Celsius air does reach the outlets of the 6×3 arrangement. The solution for the 6×3 arrangement suggests that the average air velocity at outlet pipe 6 is 14.1 m/s, while it is only 3.8 m/s for outlet pipe 1. The experience with differences between the physical system and the 0 Pa outlet gauge pressure model in the 3×3 arrangement, suggests the difference in these velocities from the model is greatly overstating the reality of the physical system. If the air velocity is thus truly lower out to outlet pipe 6, it can be expected that greater cooling occurs along the manifold, and thus it is possible that there is negative degree Celsius air reaching at least outlet pipe 6 of the 6×3 arrangement. To further support this concern, it is worth noting that the temperature profile over the third outlet pipe of the 3×3 arrangement with the adjusted

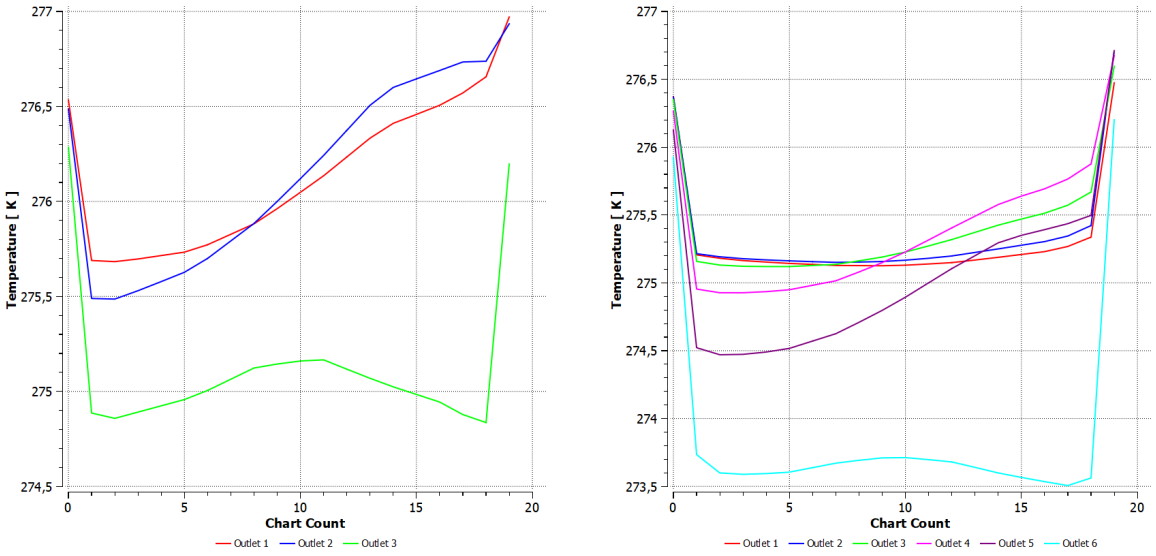

(a) 3 x 3 arrangement

(b) 6 x 3 arrangement

Figure 14: Temperature across outlet pipes at 100 cm

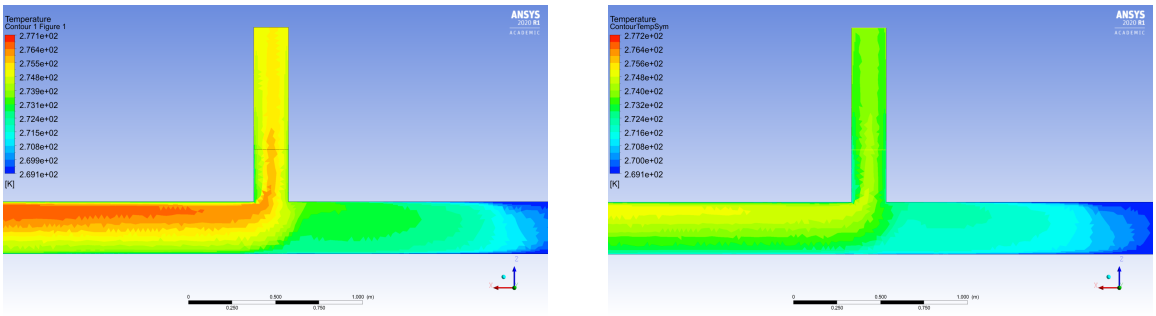

(a) 3 x 3 arrangement, centered on the 3^{rd} outlet pipe

(b) 6 x 3 arrangement, centered on the 6^{th} outlet pipe

Figure 15: Contour of temperature over symmetry plane at given T-junctions

outlet gauge pressures (data not shown) has a minimum of ca. 274.65 - a value lower than the 0 Pa outlet gauge pressure model shown in figure 14.

Given the energy cost of this system is important to the users, it would interesting to develop the analysis further along the lines of reducing the electricity inputs; be it a lower fan speed or a lower temperature. Further, it would be of value to know what the ventilation/ heating system can achieve when the store is subjected to its most extreme and economically catastrophic conditions of ambient air temperature of less than -10°C.

4 Conclusions and Outlook

We have considered a ventilation system that is under development and of high interest for sugar beet growers in Sweden and Denmark given its potential to deliver large economic value. From this, we have considered two separate cases; Air velocity, and Heat transfer. In the Air velocity case, we were able to test the importance of the method used in discretization and solving the system. This analysis showed that in general, the $k - \epsilon$ model works best while the RSM model gives the least accurate results, even if the RSM model solver seems to be more stable. A comparison of the results of the RSM Upwind method and experimental data measured from the system in the field showed that the model was able to approximately replicate the measured data, but had a significant issue with the distribution of air velocity between the outlet pipes; namely, it returned the inverse pattern to that of the experimental data. However, given the accuracy of the model at a macro level and the fact the system sits symmetrically within a sugar beet clamp, it is possible to take these results to the next step in the development of the system - modelling airflow through the clamp itself.

In the heat transfer case, we were able to run a mesh independence analysis, concluding that the mesh that was at the limits of the Academic licence was most likely of sufficiently high resolution. For the particular case tested, it was concluded that it is possible to heat -4°C air to 4°C air and that this air would not return to a sub-zero degree Celsius temperature as it passed through the system. The heat transfer case study has not actually been implemented in the field, but the results have already been communicated to the research group and have raised great interest. The case again showed the value of applying CFD to real-life systems.

The biggest challenge in both cases was the computational limitations. Even though we had access to the full ANSYS version, the computations were very heavy due to the size of the geometry. This issue could have not been resolved by scaling the geometry.

References

[1] NBR Nordic Beet Research Foundation. Air velocity data from project 604: Ventilerad lagring, EIP. Not published, 29 April 2020.

[2] H. Zhang, X. Li, Y. Wang, J. Yao, Y. Kang, and Y. Wang. Evaluation and analysis of internal flow field uniformity in grain stack based on multi zone model of porous media. *Procedia Engineering*, 205:2164–2170, 2017.